ACS APPLIED MATERIALS & INTERFACES
Research Article
www.acsami.org

Colloidal Stripe Pattern with Controlled Periodicity by Convective Self-Assembly with Liquid-Level Manipulation

Yasushi Mino, Satoshi Watanabe, and Minoru T. Miyahara*

Department of Chemical Engineering, Kyoto University, Katsura, Nishikyo, Kyoto 615-8510, Japan

Supporting Information

ABSTRACT: We describe a template-free technique for arranging colloidal particles into a stripe pattern on a large scale. A simple liquid-level manipulation system was incorporated into the vertical-deposition convective self-assembly (CSA) technique. By periodically pumping a colloidal dispersion out of or into a reservoir to manipulate the liquid level, we successfully fabricated stripe patterns with various periodicities (i.e., line widths and spacings) that are unachievable with the normal CSA technique. We developed a simple model to predict the periodicity of the resultant colloidal stripes that enables the tailored fabrication of colloidal stripes with the desirable periodicity for a practical application. This technique has the advantages of versatility and scalability. By combining this technique with the two-step CSA technique (Mino et al., *Langmuir* **2011**, *27*(9), 5290−5295), we fabricated a large-sized colloidal grid network pattern of silver nanoparticles.

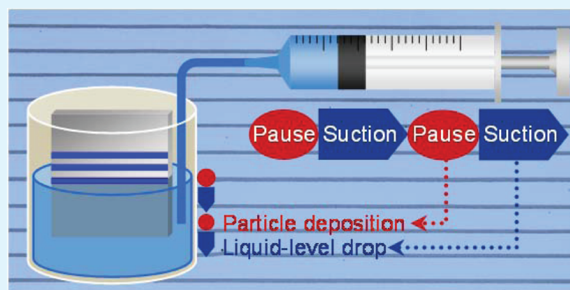

KEYWORDS: *colloid, convective self-assembly, vertical deposition, self-organization, template-free technique, stripe pattern*

INTRODUCTION

Over the past decade, two- and three-dimensional (2D and 3D) colloidal arrays have attracted considerable attention because of their wide variety of applications as photonic band gap materials,[1−3] chemical and biosensors,[4−6] media for macromolecular separation,[7,8] antireflective coatings,[9,10] superhydrophobic surfaces,[11] masks for colloidal lithography,[12−15] and so on. Several elegant fabrication methods have previously been developed for creating 2D and 3D colloidal arrays, including gravitational sedimentation,[16,17] Langmuir−Blodgett assembly,[18−20] electric-field-assisted assembly,[11,21] and spin coating.[22,23] In addition to uniform colloidal arrays, patterned structures of colloidal particles have also been intensively explored to expand the possible applications of colloidal arrays. Topographically[24,25] or chemically[26,27] patterned templates have been widely utilized to assist in the arrangement of particles into various colloidal patterns. Although template-assisted approaches can be used to fabricate desired patterns, they are generally difficult to apply to large-scale fabrication with a few exceptions,[28] and require additional processes for preparing the templates. Although several template-free techniques[29,30] have prepared colloidal patterns, the control of resultant patterns is still difficult. The establishment of a template-free technique is thus required to fabricate and control colloidal patterns on a large scale.

Convective self-assembly (CSA)[31,32] provides simple, scalable, and inexpensive routes for the fabrication of colloidal patterns as well as the formation of uniform particulate films. In this process, a hydrophilic substrate is immersed in a colloidal dispersion, and the dispersed particles are transported to the meniscus edge by the convection that compensates for the solvent evaporation from a drying region. The particles then form a hexagonally close-packed colloidal array owing to the lateral capillary forces acting between them. In our previous study, we utilized the CSA technique and successfully fabricated striped colloidal arrays without any templates.[33] The colloidal stripes exhibited well-ordered periodicity with line widths and spacings on the order of micrometers. Furthermore, we proposed the following stripe formation model. When the particle concentration of a dispersion is fairly low, the number of particles carried to the meniscus edge is so small that the growth rate of the particulate film is slower than the rate at which the liquid level falls. As the evaporation progresses, this rate difference increases the distance between the growing front of the particulate film and the liquid level, and the meniscus is gradually stretched into a concave shape. After a certain period, the stretched meniscus spontaneously breaks and slides down, resulting in the formation of particulate lines and spaces. One of the characteristics of the resultant stripe patterns is that the spacing between particulate lines is dependent on the thickness of the particulate lines.[33] In other words, the achievable periodicity of stripe patterns, i.e., the possible combinations of line widths and spacings, is naturally limited by the particle size and the number of layers. However, it is necessary to tune the line width and spacing to achieve a desirable periodicity for practical applications, such as transparent conductive films, micro fluidics, and sensor arrays. For example, for the tailored fabrication of a transparent conductive film, the line width should be tuned for its conductivity, and at the same time the control of the line spacing is necessary for its

Received: March 26, 2012
Accepted: May 29, 2012
Published: May 29, 2012

© 2012 American Chemical Society

transparency. Recently, to overcome this structural limitation, several research groups have introduced new approaches to the CSA process and actively controlled the slip motion of the meniscus tip.[34−37] Diao et al. first demonstrated the formation of nanoparticle wires on a substrate immersed vertically in a dispersion by rapidly removing a small quantity of the dispersion so as to drop the meniscus edge to a new level.[34] Huang et al. achieved selective positioning of nanowire arrays with controllable packing densities and spacings by pulling up a substrate periodically with a programmable mechanical dipper.[35] Kim et al. utilized horizontal CSA and withdrew the meniscus periodically, fabricating well-defined stripe and grid patterns of nanoparticles.[36] Their work was followed by a similar approach in which Farcau et al. periodically translated a substrate instead of withdrawing the meniscus.[37] Although they achieved control of the stripe widths and spacings, the understanding of the relationship between the operating parameters and the resultant structures has not yet been sufficient to fully control the stripe periodicity.

In the present study, we incorporate liquid-level manipulation (LLM) into vertical-deposition CSA to control the contact line motion by pumping the colloidal dispersion out of its reservoir. Although the LLM technique is the same as the substrate withdrawal method in terms of the substrate motion relative to the liquid level, the LLM can easily be integrated into the CSA process just by using an inexpensive syringe pump. Another advantage of the CSA-LLM technique is stable operation, because the substrate is disconnected from the driving motor of the pump, in contrast to the case for substrate withdrawal. In addition to the suction of the dispersion to lower the liquid level, the basic idea of which is similar to that of the method proposed by Diao et al., we newly introduce an injection operation to raise the liquid level, which will expand our capability for structural control.

The purpose of the present work is to establish a new CSA technique for tailored fabrication of colloidal stripes. By using the convective self-assembly with liquid-level manipulation (CSA-LLM) technique, we fabricate various colloidal stripe patterns composed of silica particles. We systematically examine how to control the stripe width and spacing by varying several operating parameters, and develop a simple model to predict the resultant periodicity. Furthermore, taking advantage of the versatility and scalability of the CSA-LLM technique, we combine this method with the two-step CSA technique[38] and fabricate a large-scale grid network pattern composed of silver nanoparticles.

■ EXPERIMENTAL SECTION

Materials. Silica particles with a diameter of 120 nm (Spherica Slurry 120) were purchased as an aqueous dispersion from Catalysts & Chemicals Ind. Co., Ltd., Japan. Silver nanoparticles with diameters of 10−15 nm dispersed in water (Finesphere SVW001) were purchased from Nippon Paint Co., Ltd., Japan. Here, the diameters were reported values by the manufacturers. The dispersions were diluted to a desired particle concentration with ultrapure water with a resistivity of 18 MΩ·cm obtained from a Direct-Q 3 UV Water Purification System (Millipore Corp., Bedford, MA). Micro cover glasses with dimensions of 18 × 18 mm^2 (Matsunami Glass Ind., Ltd., Japan) were used as substrates. As a preliminary cleaning procedure, the glass substrates were washed with acetone (99.5%, Kishida Chemical Co., Ltd., Japan), ethanol (99.5%, Kishida Chemical Co., Ltd., Japan), and the ultrapure water in an ultrasonic bath. Then, they were dried with compressed air and treated with a plasma cleaner (Harrick Plasma Inc., NY) to increase their hydrophilicity immediately before use.

Convective Self-Assembly with Liquid-Level Manipulation (CSA-LLM). Figure 1 illustrates a schematic of the experimental setup.

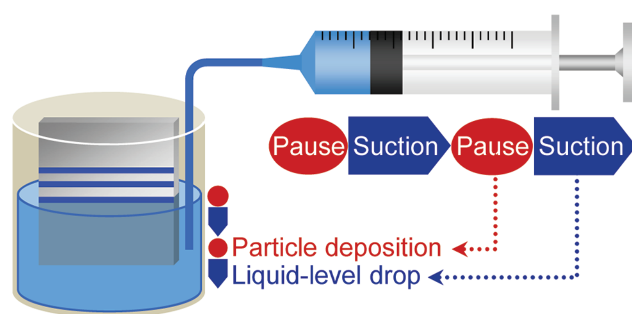

Figure 1. Schematic illustration of the convective self-assembly with liquid-level manipulation (CSA-LLM) technique.

A 20 mL beaker was filled with a dispersion with an adjusted particle concentration ϕ [vol/vol] and placed in a temperature-controlled incubator (Yamato Scientific Co., Ltd., Japan). The humidity in the incubator was measured to be less than 10% during the assembly experiments. The temperature in the incubator was set to be $T = 60$ °C, unless otherwise stated. We measured the amount of solvent that evaporated during a certain period of time and calculated the solvent evaporation rate v_e to be 0.28 ± 0.01 μm/s at $T = 60$ °C. A hydrophilic glass substrate was vertically immersed in the dispersion and kept stationary to progress the particle assembly, which is driven by the evaporation-induced convection toward the meniscus tip. At a certain interval, the dispersion was pumped out of or into the reservoir by a 5-mL syringe (Terumo Corp., Japan) installed on a programmable syringe pump (Nexus 3000, Chemyx Inc., TX) to manipulate the liquid level. We varied the amount of liquid removed in each suction operation V_p [mL] and the period between suctions τ_p [s]. The suction amount V_p is converted to a liquid-level drop distance using the formula λ_p [μm] = V_p/S, where S is the surface area of the dispersion in the beaker, that is, the cross-sectional area of the beaker minus those of the substrate and a microtube. The period between suctions represents the period of particle deposition. The rate at which the liquid level drops was set to be 90 μm/s in the present work. Note that we confirmed that varied dropping rates within the range from 10 to 200 μm/s did not affect resultant structures.

After the particle deposition, all samples were observed with a digital microscope (VHX-VK-600, Keyence Corp., Japan). The microstructures of the patterns were studied with a field-emission scanning electron microscope (JSM-6700F, JEOL Ltd., Japan).

■ RESULTS AND DISCUSSION

Stripe Formation. Figure 2a shows a conceptual graph of the liquid-level variation against time in the CSA-LLM technique. While the pump is paused, dispersed particles assemble to form a particulate line, and the liquid level falls gradually due only to the solvent evaporation (section I in Figure 2a). After a certain period (period of particle deposition τ_p [s]) the dispersion is pumped out and the liquid level quickly drops (liquid-level drop distance λ_p [μm]), thereby terminating the particulate line growth (section II in Figure 2a). Because the drop of the liquid level is quick enough to prevent the contact line from being pinned, particles are not deposited on the substrate during the liquid-level drop, resulting in the formation of a space. After the suction, the contact line is pinned again, and the next particulate line starts to form (section III in Figure 2a). Figure 2b shows an optical micrograph of a typical stripe pattern obtained from a silica dispersion of $\phi = 3.0 \times 10^{-5}$ using the CSA-LLM technique. The sets of particulate lines and subsequent spaces labeled as i and ii were fabricated with different combinations of the two operating parameters, (τ_p, λ_p) = (60 s, 40 μm) and (120 s, 70 μm). Each line is composed of a hexagonally close-packed particulate monolayer, as shown in Figure S1 (see the Supporting

dx.doi.org/10.1021/am300526g | ACS Appl. Mater. Interfaces 2012, 4, 3184−3190

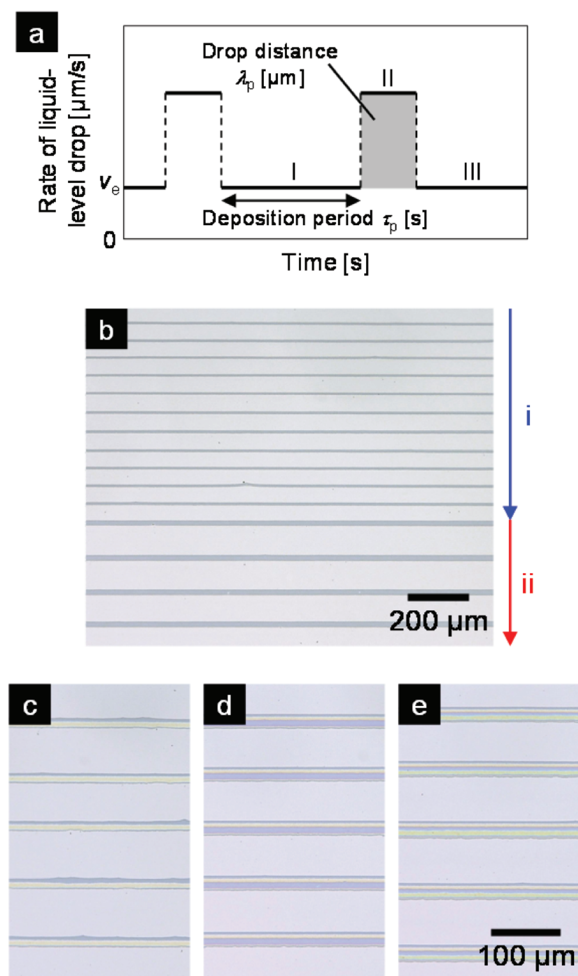

Figure 2. (a) Conceptual graph of the liquid-level variation against time in the CSA-LLM technique. (b) Optical micrograph of a typical stripe pattern obtained from a 120 nm silica dispersion of $\phi = 3.0 \times 10^{-5}$ by CSA-LLM. The sets of particulate lines and subsequent spaces labeled as i and ii were fabricated with different combinations of the two operating parameters, (τ_p, λ_p) = (60 s, 40 μm) and (120 s, 70 μm). (c−e) Optical micrographs of multilayer stripe patterns fabricated at 50 °C by CSA-LLM. In these optical micrographs, the color of the particulate lines comes from light interference and varies depending on the number of particle layers. (c) Bilayer, $\phi = 5.0 \times 10^{-5}$, (τ_p, λ_p) = (60 s, 70 μm). (d) Trilayer, $\phi = 1.0 \times 10^{-4}$, (τ_p, λ_p) = (120 s, 70 μm). (e) Four-layer, $\phi = 1.0 \times 10^{-4}$, (τ_p, λ_p) = (180 s, 70 μm).

Information). A longer τ_p clearly gives wider particulate lines, while a longer λ_p gives wider line spaces, demonstrating our ability to control the periodicity of the stripe patterns using the CSA-LLM technique. Furthermore, the CSA-LLM technique can be used to produce well-ordered multilayer stripe patterns (Figure 2c−e) as well as monolayer stripes simply by using dispersions with a high particle concentration and changing τ_p. The thickness of particulate stripes increases with a particle concentration (Figure 2c, d, from bilayer to trilayer) and also a deposition period (Figure 2d, e, from trilayer to four-layer), because a higher concentration and a longer deposition period can transport more particles into the contact line.

Another advantage of the CSA-LLM technique is that particulate lines can be produced that are narrower than those obtained using the normal CSA (without LLM). In the normal CSA technique, the line width is generally controlled only by the particle concentration of the colloidal dispersion, which accordingly requires the use of a dispersion with a fairly low particle concentration to fabricate narrow particulate lines. However, the problem is that the resultant stripes turn out to be wavy (Figure 3a), because the small number of particles carried

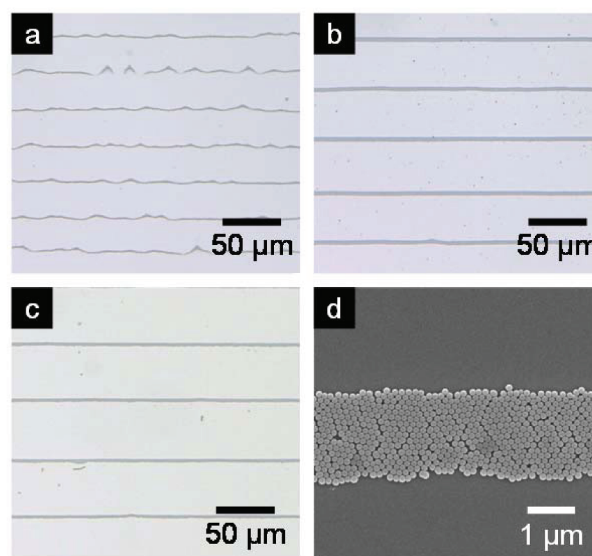

Figure 3. Optical micrographs of stripe patterns obtained from 120 nm silica dispersions of (a) $\phi = 3.0 \times 10^{-6}$ and (b) $\phi = 5.0 \times 10^{-6}$ by normal CSA (without LLM). (c) Optical micrograph and (d) SEM image of a stripe pattern fabricated from a 120 nm silica dispersion of $\phi = 2.0 \times 10^{-5}$ by CSA-LLM with τ_p = 15 s and λ_p = 50 μm.

to the meniscus edge cannot pin the contact line firmly. In the case of the stripe formation using 120 nm silica particles, the minimum line width was found to be >4 μm, which resulted from the use of a dispersion of $\phi = 5.0 \times 10^{-6}$ (Figure 3b). In the CSA-LLM process, by contrast, the deposition period τ_p as well as the particle concentration control the line width, and we can thus avoid this problem by using a particle concentration high enough to pin the contact line firmly and setting τ_p to be short. Figures 3c,d shows an example of the stripes fabricated from a dispersion of $\phi = 2.0 \times 10^{-5}$ with τ_p= 15 s. The resultant stripes are straight and measured to be ∼2 μm wide, and the hexagonally close-packed structure remained unchanged. In this manner, the CSA-LLM technique enables the periodicity of the stripe pattern to be modulated by using a single set of parameters, τ_p and λ_p.

Controlling Line Width. We also examined the effect of the period of particle deposition τ_p on the particulate line width. Figure 4 shows the relation between τ_p and the line width for stripe patterns obtained using different particle concentrations, $\phi = 1.0 \times 10^{-5}$, 2.0×10^{-5}, and 5.0×10^{-5}, with a fixed drop distance of λ_p = 50 μm. The number of layers of particulate lines is indicated by a number beside each plot. Note that the plot at $\phi = 5.0 \times 10^{-5}$ and τ_p = 30 s has two numbers, which means that the stripes are partially bilayer, as shown in Figure S2 of the Supporting Information. The line width increases almost proportionally with τ_p, and the slope, or the rate of particulate line growth, is larger for higher particle concentrations. This is natural, because a longer τ_p and the higher particle concentration transport more particles to the contact line during the deposition period. At $\phi = 5.0 \times 10^{-5}$, an increase in the number of layers results in a decrease in the slope; this is because the formation of a bilayer particulate film requires twice as many particles as monolayer formation. It should be noted that the linear relation

 dx.doi.org/10.1021/am300526g | ACS Appl. Mater. Interfaces 2012, 4, 3184−3190

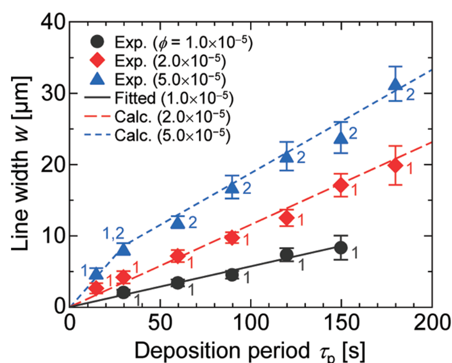

Figure 4. Relation between the deposition period τ_p and the line width w of stripe patterns fabricated from 120 nm silica dispersions of different particle concentrations, $\phi = 1.0 \times 10^{-5}$, 2.0×10^{-5}, and 5.0×10^{-5}, at $\lambda_p = 50$ μm. The solid line is a fitted line, whereas the dotted ones are the results calculated using eq 2.

with time is confined to a limited deposition period τ_p because a larger τ_p, such as $\tau_p = 180$ s under the condition of $\phi = 1.0 \times 10^{-5}$, results in a biperiodic stripe pattern in which thick and thin stripes form alternately, as shown in Figure S3 of the Supporting Information. The threshold length of the deposition period increases with the particle concentration. The details of the biperiodic stripe formation are described in the caption of Figure S3 in the Supporting Information.

These results show the same trend as the results obtained for the formation of particulate continuous films by the normal CSA, in which the rate of the particulate film growth is almost proportional to the particle concentration of the dispersion and inversely proportional to the number of layers. We thus suppose that the model of particulate continuous film formation proposed by Dimitrov and Nagayama[39] and Prevo and Velev[40] is applicable to the stripe formation in the CSA-LLM process. A simple mass balance around the thin drying film can be used to express the growth rate of a colloidal film v_c as[39]

$$v_c = \frac{\beta j_e l \phi}{h(1-\varepsilon)(1-\phi)} \tag{1}$$

Here, β is a parameter that relates the mean solvent velocity to that of the particles and varies from 0 to 1. β depends on the particle–particle and particle-substrate interactions and particle concentration, and we can assume it to be 1 for a repulsive and dilute system containing small particles used in our experiments. j_e is the rate of solvent evaporation per unit of drying length, l is the drying length, and h and ε are the height and the porosity of the deposited colloidal film. Assuming that particulate films are composed of hexagonally close-packed colloidal particles, we can replace $h(1-\varepsilon)$ with $0.605kd$, where k is the number of layers and d is the diameter of the colloidal particles. Furthermore, by lumping the term $\beta j_e l$ into a single parameter, K, we can express the particulate line width w as[40]

$$w = \sum_{i=1}^{k} v_{c,i}\tau_{p,i} = \sum_{i=1}^{k} \frac{K\phi}{0.605id(1-\phi)}\tau_{p,i} \tag{2}$$

Here, $v_{c,i}$ is the growth rate of a colloidal i-layer film, whereas $\tau_{p,i}$ is the period of time for the i-layer film formation and $\tau_p = \sum_{i=1}^{k} \tau_{p,i}$. For a given K, eq 2 can predict the particulate line width, although a theoretical basis for estimating a K value has not yet been established. Here, we obtained K experimentally by using the data at $\phi = 1.0 \times 10^{-5}$. From the slope of the solid straight line from the origin in Figure 4, we evaluated $K = 4.2 \times 10^2$ μm^2/s. Because K predominantly depends on the temperature and humidity, the same K value should apply to the other concentrations. For $\phi = 5.0 \times 10^{-5}$, we assumed that the number of layers increases from $k = 1$ to 2 at $\tau_p = 30$ s when bilayer lines started to form (Figure S2 in the Supporting Information), which means $\tau_{p,2} = \tau_p - 30$ s. The calculated values are plotted as dotted lines in Figure 4 and exhibit fairly good agreement with our experimental data, demonstrating that the simple mass balance model accurately captures the deposition process of the CSA-LLM technique.

Controlling Line Spacing. The line spacing is mainly governed by the liquid-level drop distance. Figure 5a shows the

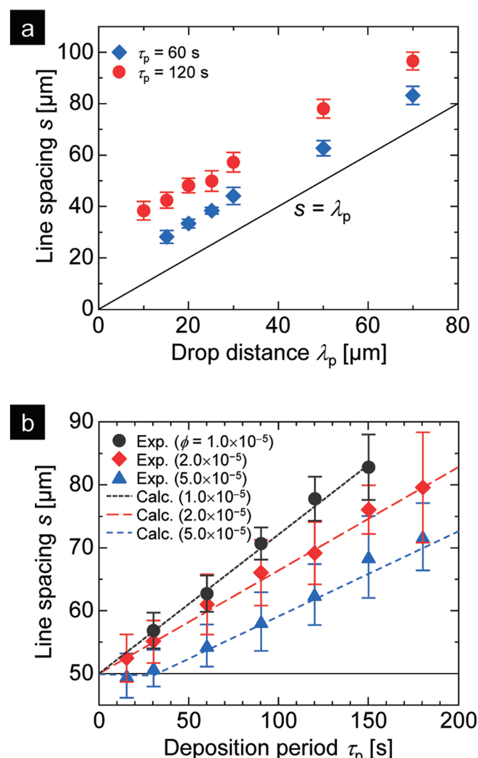

Figure 5. (a) Relation between the drop distance λ_p and the line spacing s of stripe patterns fabricated from a 120 nm silica dispersion of $\phi = 1.0 \times 10^{-5}$ for different deposition periods $\tau_p = 60$ and 120 s. The solid line represents $s = \lambda_p$. (b) Relation between the deposition period τ_p and the line spacing s of stripe patterns fabricated from 120 nm silica dispersions of different particle concentrations, $\phi = 1.0 \times 10^{-5}$, 2.0×10^{-5}, and 5.0×10^{-5}, at $\lambda_p = 50$ μm. The solid line shows $s = \lambda_p = 50$ μm, and the dotted lines show the results calculated using eq 3.

line spacing s of stripe patterns produced from silica dispersions of $\phi = 1.0 \times 10^{-5}$ for different τ_p values as a function of the liquid-level drop distance λ_p. One would expect the line spacing s to be equal to λ_p, as indicated by the solid line in Figure 5a. However, the resultant s shows a positive parallel shift in the y-direction, and, furthermore, the longer deposition period τ_p of 120 s results in a wider s than does $\tau_p = 60$ s, suggesting that s depends on τ_p. To show more details about the effect of τ_p, the stripe spacings s produced with $\lambda_p = 50$ μm are plotted as a function of τ_p for different particle concentrations of $\phi = 1.0 \times 10^{-5}$, 2.0×10^{-5}, and 5.0×10^{-5} in Figure 5b, where the solid line shows $s = \lambda_p = 50$ μm. The line spacing increases linearly with the deposition period, the slope is larger for lower particle concentrations, and, for the results obtained with $\phi = 5.0 \times 10^{-5}$, an increase in the number of layers increases the slope.

These results are attributable to the rate difference between the solvent evaporation v_e and the particulate line growth v_c, as illustrated in Figure 6. Here, we explain the formation process by

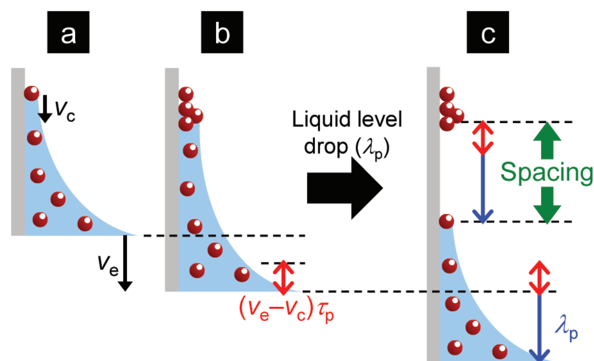

Figure 6. Schematic illustrations of the particle deposition process in CSA-LLM. (a) A particulate line steadily grows at a rate v_c, whereas the solvent evaporation lowers the liquid level at a rate v_e. Under the fairly low concentration conditions used in the present work, v_c can be slower than v_e. After a deposition period τ_p, (b) the meniscus is accordingly stretched by $(v_e - v_c)\tau_p$, and consequently, (c) the spacing is wider by $(v_e - v_c)\tau_p$ than the liquid-level drop λ_p.

using v_c instead of $v_{c,i}$ for simplicity. During a deposition period τ_p, a particulate line steadily grows at a rate v_c, while the solvent evaporation lowers the liquid level at a rate v_e. For the fairly low concentration conditions used in the present work, v_c is slower than v_e because only a small number of particles are transferred to the contact line by the convective flows (Figure 6a). The meniscus is accordingly stretched by $(v_e - v_c)\tau_p$, as shown in Figure 6b, and, consequently, the spacing s is wider by $(v_e - v_c)\tau_p$ than the liquid-level drop distance λ_p caused by the suction of the dispersion. Because v_c is a function of the particle concentration ϕ and the number of layers k, as in eq 2, the $(v_e - v_c)\tau_p$ term explains the dependence of the line spacing well, as shown in Figure 5b. Quantitatively, the line spacing s can be expressed as

$$s = \sum_{i=1}^{k} (v_e - v_{c,i})\tau_{p,i} + \lambda_p = v_e\tau_p - \sum_{i=1}^{k} \frac{K\phi}{0.605id(1-\phi)}\tau_{p,i} + \lambda_p \qquad (3)$$

We calculated the line spacing with eq 3 using $K = 4.2 \times 10^2\ \mu m^2/s$, which was obtained in the previous section. The calculated spacing shown by the dotted lines in Figure 5b agrees fairly well with the experimental results.

As described above, the line spacing can easily be expanded just by sucking out a larger amount of the dispersion. In contrast, upon narrowing the spacing, we found out that there seemed to be a lower limit to the spacing. The critical spacing for the 120 nm silica particles is around 30 μm, which is almost the same as that achieved by the spontaneous formation without LLM. A smaller amount of suction did not produce a narrower spacing, because the liquid-level drop caused by the suction was not enough to induce the slip of the meniscus tip, resulting in wider lines and spacings than expected. This result suggests that the meniscus can be stretched to a certain critical length by the liquid-level drop, and this critical length defines the minimum width of the spacing. To avoid this problem, our idea is to raise the liquid level immediately after the suction. Figure 7a shows a conceptual graph of the liquid-level variation against time. After the particulate line formation (see section I in Figure 7a), the liquid level is quickly dropped to cut off the meniscus (section II in Figure 7a) and then raised by the injection of the dispersion (section III in Figure 7a), followed by the next line deposition (section IV in Figure 7a). The resultant spacing can be expected to be $s = (v_e - v_c)\tau_p + \lambda_p - \lambda_p'$, where λ_p' is the distance of the liquid-level rise.

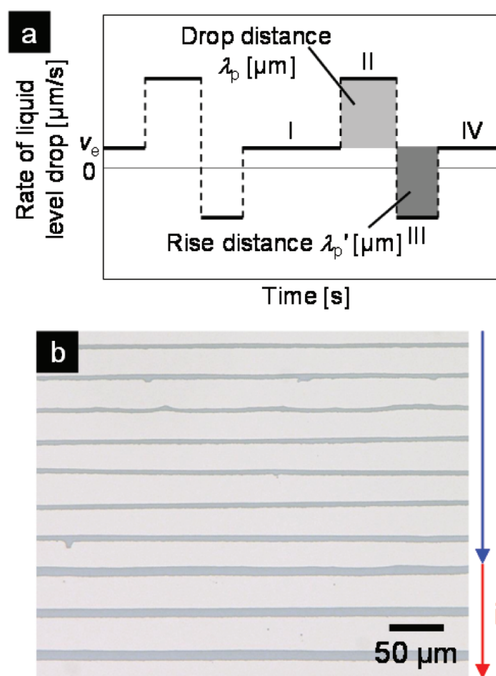

Figure 7. (a) Conceptual graph of the liquid-level variation against time used to narrow the line space. (b) Optical micrograph of a stripe pattern fabricated from a 120 nm silica dispersion of $\phi = 2.0 \times 10^{-5}$ at $\tau_p = 65$ s, $\lambda_p = 100\ \mu$m, and $\lambda_p' = 90\ \mu$m. The stripes labeled as i were obtained using the combination of the liquid-level drop and rise, whereas the stripes labeled as ii were fabricated using the normal CSA without LLM.

Figure 7b shows an optical micrograph of a resultant stripe pattern fabricated from a silica dispersion of $\phi = 2.0 \times 10^{-5}$ at $\tau_p = 65$ s, $\lambda_p = 100\ \mu$m, and $\lambda_p' = 90\ \mu$m. The stripes obtained using the combination of the liquid-level drop and rise exhibit narrower spacings (~24 μm, labeled as i) than those of stripes formed using the normal CSA without LLM (labeled as ii). Note that the widths of lines (i) are narrower than those of lines (ii) because the growth of lines (i) was terminated by the liquid-drop operation in the middle of the particulate line formation. At present, the minimum spacing obtained so far is >20 μm, and further narrowing is still a challenge, because increasing λ_p' can result in the merging of two consecutive particulate lines. More precise manipulation would thus be needed. However, this result at least demonstrates that our technique allowed us to successfully break the threshold minimum spacing in a controlled manner by performing an injection right after the suction of the dispersion.

Versatility and Scalability. In addition to providing easy control of the stripe width and spacing, the CSA-LLM technique also allows the fabrication of uniform patterns with fewer structural defects and distortions than are observed for the normal CSA because of its precisely programmed operation, which enables quick and large-scale fabrication. Furthermore, this technique can be applied to various types of particles unless the particles are so large that they easily settle out, and is applicable to not only hydrophilic but partially wettable

substrates of the contact angle of less than 35°. We can thus easily extend our technique to the fabrication of grid patterns by combining it with the two-step CSA technique.[38] To demonstrate the performance of this combined technique, we arranged 10−15 nm silver nanoparticles into a grid network on a flexible substrate (polyethylene terephthalate; PET) with dimensions of 5 cm ×5 cm, which is shown in Figure 8.

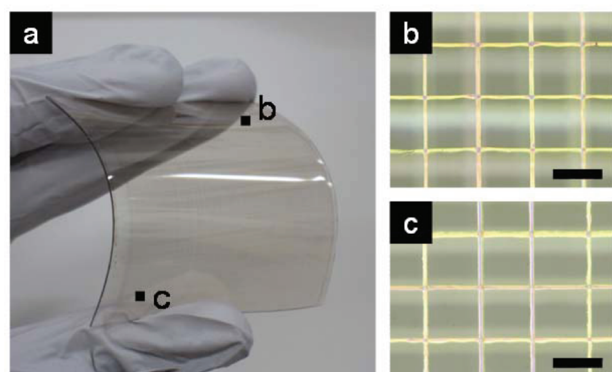

Figure 8. (a) Photograph and (b, c) optical micrographs of a large-sized grid network pattern of silver nanoparticles that was fabricated on the 5 cm × 5 cm PET substrate from a 10−15 nm silver nanoparticle dispersion of $\phi = 1.0 \times 10^{-5}$ by combining the CSA-LLM technique with the two-step CSA technique. Scale bars are 200 μm.

The resultant grid structure is well-defined and uniform over the whole substrate, as shown in the magnified images (Figure 8b, c). It should be noted that this grid pattern of silver nanoparticles was able to keep its pattern after several bending trials of the substrate. We believe that the CSA-LLM technique has potential for various applications because of its versatility and scalability.

■ CONCLUSIONS

We investigated a process for forming striped colloidal arrays by using the convective self-assembly (CSA) technique with liquid-level manipulation (LLM), in which we quickly lowered or raised the liquid level by pumping a colloidal dispersion out of or into a reservoir at a certain regular interval. We demonstrated that our technique can be used to fabricate stripe patterns with various periodicities, i.e., particulate line widths and spacings, that are unachievable using the normal CSA without LLM. The particulate line width linearly increased with the time during which the pump was at rest. Although the liquid-level drop created the space between two lines, the spacing turned out to be wider than the drop distance, which was attributable to the lowering of the liquid level caused by the solvent evaporation. We applied a model formula that was originally proposed for continuous film formation to the stripe pattern formation and confirmed that the equation shows quantitative agreement with the experimentally obtained stripe width. We developed a simple equation based on the stripe formation mechanism to predict the stripe spacing and also demonstrated that the equation exactly predicts the resultant spacing.

Furthermore, by combining our technique with the two-step CSA technique, we successfully fabricated a large-sized grid network pattern of silver nanoparticles. The CSA-LLM is thus a simple, inexpensive, and versatile technique for fabricating colloidal stripe and grid patterns with a desired periodicity and is believed to have the potential for technological applications in a variety of fields. Although we did not explore the temperature effects in this study, we obtained a qualitative trend that the growth rate of a particulate film increases with the temperature because a higher temperature accelerates the solvent evaporation and thus transports more particles into the contact line, which enables us to speed up the CSA-LLM process. Now, we are working on this topic and will discuss it in a future publication.

■ ASSOCIATED CONTENT

Supporting Information

SEM image of the particulate line shown in Figure 2b. Optical micrograph of a stripe pattern obtained from a silica dispersion of $\phi = 5.0 \times 10^{-5}$ by CSA-LLM with $\tau_p = 30$ s. Optical micrograph of a biperiodic stripe pattern obtained from a silica dispersion of $\phi = 1.0 \times 10^{-5}$ by CSA-LLM with $\tau_p = 180$ s. This material is available free of charge via the Internet at http://pubs.acs.org.

■ AUTHOR INFORMATION

Corresponding Author

*E-mail: miyahara@cheme.kyoto-u.ac.jp.

Notes

The authors declare no competing financial interest.

■ ACKNOWLEDGMENTS

This work was supported in part by a Grant-in-Aid for Young Scientists (A) from MEXT, the Global Centers of Excellence (G-COE) Program of the Japan Society for the Promotion of Science (JSPS), the Core-to-Core (CTC) Program of JSPS, and the Mizuho Foundation for the Promotion of Sciences.

■ REFERENCES

(1) Blanco, A.; Chomski, E.; Grabtchak, S.; Ibisate, M.; John, S.; Leonard, S. W.; Lopez, C.; Meseguer, F.; Miguez, H.; Mondia, J. P.; Ozin, G. A.; Toader, O.; van Driel, H. M. *Nature* **2000**, *405*, 437−440.
(2) Jiang, P.; Ostojic, G. N.; Narat, R.; Mittleman, D. M.; Colvin, V. L. *Adv. Mater.* **2001**, *13*, 389−393.
(3) Vlasov, Y. A.; Bo, X. Z.; Sturm, J. C.; Norris, D. J. *Nature* **2001**, *414*, 289−293.
(4) Holtz, J. H.; Asher, S. A. *Nature* **1997**, *389*, 829−832.
(5) Lee, Y. J.; Braun, P. V. *Adv. Mater.* **2003**, *15*, 563−566.
(6) Nakayama, D.; Takeoka, Y.; Watanabe, M.; Kataoka, K. *Angew. Chem., Int. Ed.* **2003**, *42*, 4197−4200.
(7) Zheng, S.; Ross, E.; Legg, M. A.; Wirth, M. J. *J. Am. Chem. Soc.* **2006**, *128*, 9016−9017.
(8) Zeng, Y.; He, M.; Harrison, D. J. *Angew. Chem., Int. Ed.* **2008**, *47*, 6388−6391.
(9) Prevo, B. G.; Hon, E. W.; Velev, O. D. *J. Mater. Chem.* **2007**, *17*, 791−799.
(10) Zhang, L.; Qiao, Z.-A.; Zheng, M.; Huo, Q.; Sun, J. *J. Mater. Chem.* **2010**, *20*, 6125−6130.
(11) Joung, Y. S.; Buie, C. R. *Langmuir* **2011**, *27*, 4156−4163.
(12) Haynes, C. L.; Van Duyne, R. P. *J. Phys. Chem. B* **2001**, *105*, 5599−5611.
(13) Wang, X. D.; Summers, C. J.; Wang, Z. L. *Nano Lett.* **2004**, *4*, 423−426.
(14) Xia, D. Y.; Ku, Z. Y.; Li, D.; Brueck, S. R. J. *Chem. Mater.* **2008**, *20*, 1847−1854.
(15) Garnett, E.; Yang, P. D. *Nano Lett.* **2010**, *10*, 1082−1087.
(16) Mayoral, R.; Requena, J.; Moya, J. S.; Lopez, C.; Cintas, A.; Miguez, H.; Meseguer, F.; Vazquez, L.; Holgado, M.; Blanco, A. *Adv. Mater.* **1997**, *9*, 257−260.
(17) Wang, W.; Gu, B.; Liang, L.; Hamilton, W. *J. Phys. Chem. B* **2003**, *107*, 3400−3404.
(18) Reculusa, S.; Ravaine, S. *Chem. Mater.* **2003**, *15*, 598−605.
(19) Tao, A.; Sinsermsuksakul, P.; Yang, P. *Nat. Nanotechnol.* **2007**, *2*, 435−440.

(20) Zhu, J.; Yu, Z. F.; Burkhard, G. F.; Hsu, C. M.; Connor, S. T.; Xu, Y. Q.; Wang, Q.; McGehee, M.; Fan, S. H.; Cui, Y. *Nano Lett.* **2009**, *9*, 279−282.
(21) Zhang, K. Q.; Liu, X. Y. *Nature* **2004**, *429*, 739−743.
(22) Jiang, P.; McFarland, M. J. *J. Am. Chem. Soc.* **2004**, *126*, 13778−13786.
(23) Mihi, A.; Ocana, M.; Miguez, H. *Adv. Mater.* **2006**, *18*, 2244−2249.
(24) Cui, Y.; Bjork, M. T.; Liddle, J. A.; Sonnichsen, C.; Boussert, B.; Alivisatos, A. P. *Nano Lett.* **2004**, *4*, 1093−1098.
(25) Malaquin, L.; Kraus, T.; Schmid, H.; Delamarche, E.; Wolf, H. *Langmuir* **2007**, *23*, 11513−11521.
(26) Fustin, C. A.; Glasser, G.; Spiess, H. W.; Jonas, U. *Langmuir* **2004**, *20*, 9114−9123.
(27) Thomson, N. R.; McLachlan, M. A.; Bower, C. L.; McComb, D. W. *Langmuir* **2009**, *25*, 11344−11350.
(28) Junkin, M.; Watson, J.; Geest, J. P. V.; Wong, P. K. *Adv. Mater.* **2009**, *21*, 1247−1251.
(29) Huang, J.; Kim, F.; Tao, A. R.; Connor, S.; Yang, P. *Nat. Mater.* **2005**, *4*, 896−900.
(30) Xu, J.; Xia, J.; Lin, Z. *Angew. Chem., Int. Ed.* **2007**, *46*, 1860−1863.
(31) Denkov, N.; Velev, O.; Kralchevski, P.; Ivanov, I.; Yoshimura, H.; Nagayama, K. *Langmuir* **1992**, *8*, 3183−3190.
(32) Denkov, N. D.; Velev, O. D.; Kralchevsky, P. A.; Ivanov, I. B.; Yoshimura, H.; Nagayama, K. *Nature* **1993**, *361*, 26.
(33) Watanabe, S.; Inukai, K.; Mizuta, S.; Miyahara, M. T. *Langmuir* **2009**, *25*, 7287−7295.
(34) Diao, J. J.; Sun, J.; Hutchison, J. B.; Reeves, M. E. *Appl. Phys. Lett.* **2005**, *87*, 103113.
(35) Huang, J.; Fan, R.; Connor, S.; Yang, P. *Angew. Chem., Int. Ed.* **2007**, *46*, 2414−2417.
(36) Kim, H. S.; Lee, C. H.; Sudeep, P. K.; Emrick, T.; Crosby, A. J. *Adv. Mater.* **2010**, *22*, 4600−4604.
(37) Farcau, C.; Sangeetha, N. M.; Moreira, H.; Viallet, B.; Grisolia, J.; Ciuculescu-Pradines, D.; Ressier, L. *ACS Nano* **2011**, *5*, 7137−7143.
(38) Mino, Y.; Watanabe, S.; Miyahara, M. T. *Langmuir* **2011**, *27*, 5290−5295.
(39) Dimitrov, A. S.; Nagayama, K. *Langmuir* **1996**, *12*, 1303−1311.
(40) Prevo, B. G.; Velev, O. D. *Langmuir* **2004**, *20*, 2099−2107.